*This is an Accepted Manuscript of an article published by Taylor & Francis in*

*Quantitative InfraRed Thermography Journal*

*on Volume 23, 2026 - Issue 1, available at:*
https://doi.org/10.1080/17686733.2025.2524279

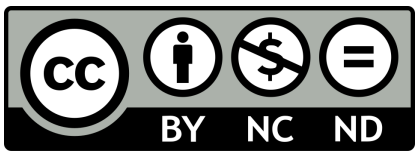

# Non-destructive assessment of crystallographic texture and mechanical behaviour in AZ31 Magnesium alloys via pulsed laser thermography

Dell'Avvocato G. [a]*, Cusanno A. [b], Bison P. [c], Rossi S [c], Palumbo G. [b], Ferrarini G [c]

[a] University of L'Aquila, Department of Industrial and Information Engineering and Economics (DIIIE), Piazzale Ernesto Pontieri 1, Monteluco di Roio - 67100 L'Aquila, Italy, giuseppe.dellavvocato@univaq.it

[b] Polytechnic University of Bari, Department of Mechanics, Mathematics and Management (DMMM), Via Edoardo Orabona - 70125 Bari, Italy, angela.cusanno@poliba.it, gianfranco.palumbo@poliba.it

[c] Institute of Construction Technologies (CNR-ITC), National Research Council of Italy – 35127, Padua, Italy, bison@itc.cnr.it, stefano.rossi@itc.cnr.it, ferrarini@itc.cnr.it

* Corresponding author: giuseppe.dellavvocato@univaq.it

## Abstract

This paper investigates the use of pulsed laser spot thermography as a non-destructive technique to evaluate mechanical properties and crystallographic texture changes in AZ31 magnesium alloys after thermal treatment. Eight AZ31 specimens were studied in two metallurgical conditions: three as-received (H24 tempered) and five annealed at 450 °C for 10,000 seconds. Thermal diffusivity was measured non-destructively using laser spot thermography, while standard destructive methods provided hardness and grain size values for reference. Results highlighted an unexpected reduction in thermal diffusivity (around 18%) after annealing, despite a notable increase in grain size (approximately 75%) and a corresponding decrease in hardness (13%). Statistical analysis showed a clear negative correlation between grain size and thermal diffusivity ($R = -0.907$, $p < 0.01$), along with a moderate positive correlation between hardness and diffusivity ($R = 0.745$, $p < 0.05$). Unlike in steels, where increased grain size usually corresponds to higher thermal conductivity, the observed diffusivity decrease in AZ31 is likely due to microstructural complexities such as texture evolution, lattice distortions, and secondary phases. The study demonstrates—for the first time—that pulsed laser thermography effectively captures microstructural changes related to mechanical behaviour and crystallographic orientation in magnesium alloys, offering a rapid, non-destructive, and reliable alternative to traditional characterization methods.

**Keywords:** Pulsed laser thermography, thermal diffusivity, crystallographic texture, non-destructive testing (NDT), mechanical behaviour, magnesium alloys (MgAZ31)

## 1. Introduction

Magnesium (Mg) is the lightest structural metal, thus Mg alloys are highly desirable for engineering applications that require minimal weight, while ensuring high strength. One of the primary sectors benefiting from Mg alloys is the transportation industry, where lightweight materials contribute significantly to improve fuel efficiency and reducing carbon dioxide ($CO_2$) emissions [1]. Additionally, thanks to the Mg biocompatibility and biodegradability in human body fluids, the use of these alloys extends to biomedical applications[2] for producing bioresorbable implants, that offer the significant advantage of eliminating the need for a second surgical procedure for removal [3,4].

The AZ31 alloy, that is the most common magnesium alloy used in industry [5], exhibits high formability at elevated temperatures, making it suitable for fabricating geometrically complex components using advanced metal forming technologies, such as hot gas forming [6] that is a flexible manufacturing process that uses gas pressure as a forming tool, acting on a heated metal sheet, forcing it to expand and copy the geometry of a die.
The advantage of low-cost equipment [7] compared to the conventional stamping is counterbalanced by the resulting large thickness variations along the profile of the geometry that can affect the performance of the component [8]. To overcome this drawback, some of the authors proposed a methodology for improving the thickness uniformity of AZ31 components produced by hot gas forming using a Mg alloy (AZ31) blank laser heat treated in a predefined area prior to forming. Thanks to the local heat treatment, the initial grain size distribution of the blank was very locally changed, thus tailoring the mechanical properties and the plastic deformation behaviour of the blank during the forming operation [9].

A central challenge remains the assessment of microstructural and mechanical properties after heat treatments such as annealing. This requires destructive testing techniques such as hardness measurements or metallographic analysis. However, grain size and hardness alone are insufficient to fully characterize mechanical behaviour in magnesium alloys with a hexagonal close-packed (hcp) structure. Due to their anisotropic crystal structure, magnesium alloys exhibit mechanical responses strongly influenced by texture—namely, the orientation of the hcp

planes [10,11]. Moreover, the presence of secondary phases and solute atoms in a solid solution introduces lattice distortions that also affect mechanical performance [12,13].

High-resolution characterization techniques such as scanning electron microscopy (SEM), electron backscattering diffraction (EBSD), energy dispersive x-ray spectroscopy (EDS) and x-ray diffraction (XRD) are typically required to evaluate these microstructural aspects properly [12,13]. These methods are both time- and cost-intensive and, being destructive, they can only be applied to sampled specimens. This is a significant limitation in biomedical applications, where components are often custom-made and produced as unique parts, making destructive testing impractical. Additionally, these techniques provide only local information, making it difficult to assess the properties of the entire component, especially in case of local heat treatment.

Non-destructive testing (NDT) techniques offer a promising alternative. While commonly used NDT methods such as tomography, ultrasound, and eddy current testing are widespread in inspection for this purpose [13–16], they still present limitations such as long inspection times, physical contact and difficulties in automation. Infrared thermography emerges as a particularly attractive solution due to its non-contact, full-field capabilities and faster acquisition and analysis times than conventional NDT methods for several applications: detection and quantitative analysis of defects [17–24], process monitoring [25–27] and material characterisation [28–31].

Several studies have shown that changes in microstructure and mechanical properties in steels are associated with variations in thermophysical properties, particularly thermal diffusivity. For instance, Mandelis et al. [32] identified an inverse correlation between hardness and thermal diffusivity. Other authors have exploited this principle to derive through-thickness hardness profiles and to explore the sensitivity of thermal effusivity [33] to similar variations. However, this behaviour cannot be generalized to all metallic materials. The mechanisms that alter mechanical properties following thermal treatment vary and do not always involve grain growth alone; they may instead stem from crystal lattice distortion, particularly in magnesium alloys.

Generally, grain growth reduces grain boundary density and facilitates heat conduction by limiting phonon scattering. However, in hcp magnesium alloys, lattice distortions—such as those induced by dislocations, solute atoms, and precipitates—can significantly affect thermal transport's electronic and phononic components[34]. A primary objective of this study is to assess whether thermal diffusivity in magnesium alloys correlates with grain size and hardness, as observed in steels, or whether lattice distortions have a counteracting effect.

This work selected pulsed laser spot thermography as a non-destructive method to measure thermal diffusivity in different states of the Mg AZ31 alloy[29,35–37]. A simple and time-efficient experimental protocol was developed to meet the requirements of industrial process integration. This study represents the first step of a broader research effort aimed at developing a thermographic NDT procedure capable of estimating mechanical properties—and even texture characteristics—of magnesium alloys through thermophysical measurements alone as also explored in recent approaches combining thermography and AI-based interpretation for anisotropic composite materials[38].

Eight Mg AZ31 specimens with a nominal thickness of approximately 1 mm were examined. Three were kept in the as-received H24 tempered condition, while the remaining five were annealed at 450 °C for 10000 s to promote static grain growth. Grain growth kinetics were expected to follow the equation proposed by Carpenter et al. [39], expressed as $d_s = (d_0^N + Ct)^{\frac{1}{N}}$, where $d_S$ and $d_0$ are the final and initial grain sizes, respectively, t is the annealing time and *C* and *N* are material-dependent constants. Two distinct material states—H24 tempered and annealed—were thus investigated.

All specimens were tested using pulsed laser spot thermography to extract through-thickness thermal diffusivity values. Metallographic and mechanical tests were performed on the same samples to measure grain size and hardness. The correlation between thermal diffusivity, grain size, and hardness was subsequently analysed.

To the best of our knowledge, this is the first work proposing a non-destructive laser thermography-based procedure for quantitatively evaluating not only the mechanical properties but also the average grain size in Mg alloys. Moreover, this study demonstrates—for the first time—the sensitivity of thermal diffusivity to crystallographic texture variations in magnesium alloys through a fully non-destructive approach.

## 2. Theory

### 2.1 Pulsed laser spot method

The well-established pulsed laser spot thermography technique [29,35–37] was adopted among the various thermographic methods for measuring thermal diffusivity in reflection configuration [40–45]. This approach relies on analysing the time evolution of the surface temperature of a body of thickness $L$, subjected to an impulsive heating event generated by a laser spot of radius $R$ with a spatial distribution typically Gaussian or top-hat. The method enables the estimation of thermal diffusivity in the in-plane ($\alpha_p$) and through-thickness ($\alpha_n$) directions [35,36,46]. The present study focuses on the latter, whose aim is to correlate the thermal diffusivity with the mechanical and microstructural properties along the thickness direction, as previously explored for boron steel in earlier works by some of the authors [28,29].

In this context, the method proves particularly robust, as the spatial non-uniformity of the laser beam does not affect the accuracy of the diffusivity measurement in the direction normal to the surface, as also confirmed in studies integrating numerical simulation and experimental thermography with advanced pre/post-processing techniques[47]. This aspect was explicitly addressed by Bison et al. [48], who demonstrated that, in a homogeneous and isotropic medium, the spatially integrated surface thermal response—that is, the integral of the surface temperature over the area affected by the heating—is independent of the specific shape of the spatial distribution of the input pulse. More specifically, in the domain of integral transforms, the zero spatial frequency component (k=0) of the Fourier–Bessel transform of the surface temperature corresponds to the spatial integral of the temperature in the space domain. Under these conditions, the system response is formally equivalent to that obtained with spatially uniform heating and matches the classical one-dimensional solution for a slab medium as shown in equation 1 in which $e$ is the thermal effusivity, $Q_0$ the amount of energy [46], $z$ is the coordinate along the slab thickness and z=0 represents the plane of the heated surface.

$$\bar{T}(t, z=0) = \frac{Q_0}{e\sqrt{\pi t}}\left(1 + 2\sum_{n=1}^{\infty} \exp\left(-\frac{n^2 L^2}{\alpha_n t}\right)\right) \tag{1}$$

Therefore, provided that the integration area is sufficiently large to cover the entire heated region, a simplified 1D model is fully justified. In particular, to determine the diffusivity in the through-thickness direction, it is sufficient to compute the average surface temperature over the heated area and perform a fitting using the analytical solution for a homogeneous medium, from which the parameter $\alpha_n/L^2$ is derived. Once the thickness is known, the thermal diffusivity can be accurately estimated.

While equation (1) describes the case of a homogeneous slab with adiabatic boundaries, in this study, data fitting was carried out using the following analytical solution for the front-surface temperature evolution of a two-layer system under instantaneous surface heating [48]:

$$\bar{T}(t, z=0) = \frac{Q_0}{e_1\sqrt{\pi t}}\left[1 + 2\sum_{n=1}^{\infty} \Gamma^n \exp\left(-\frac{n^2 L^2}{\alpha t}\right)\right] \tag{2}$$

where $\alpha$ is the thermal diffusivity, $L$ is the thickness of the first layer and $\Gamma$ is the interfacial reflection coefficient defined as:

$$\Gamma = \frac{e_1 - e_2}{e_1 + e_2} \tag{3}$$

with $e_1$ and $e_2$ being the thermal effusivities of the specimen and the backing medium, respectively [48]. The entire pre-factor $Q_0/(e_1\pi)$ is absorbed into a fitting parameter $A$, so that the model allows simultaneous estimation of $A$, $a$ and $\Gamma$ without requiring prior knowledge of heat input or effusivity.

The inclusion of the interface effect at the rear surface reflects the physical modeling required to account for non-ideal insulation at the back, even though the sample was not in contact with any substrate. In the experimental setup, the specimen was freely suspended and thermally isolated as much as possible, but slight deviations from adiabaticity may still occur at the rear surface. Conversely, heat losses at the front surface can be reasonably neglected due to the short observation time, the absence of forced convection, and the high thermal conductivity of the AZ31 magnesium alloy.

Although the reflection coefficient Γ is formally defined to describe conductive mismatch at the rear interface between the specimen and a backing medium, this work uses it as an effective fitting parameter to account for any minor deviation from the ideal adiabatic boundary condition. This includes possible residual losses from both the rear and front surfaces, even though the front side is considered adiabatic due to the short observation window, high thermal conductivity of the material, and low Biot number ($Bi < 0.02$). This assumption, for metals under short-time photothermal excitation, was further validated through a dedicated sensitivity analysis. Specifically, using the lowest fitted value of $\Gamma = 0.98$ instead of $\Gamma = 1.00$ caused a variation in the estimated thermal diffusivity $a$ of less than 0.6%, confirming that any deviation from ideal adiabatic conditions at the rear has a negligible effect on the extracted α.

Therefore, due to the consistently high values of $\Gamma$ obtained in this work (always $> 0.98$), the simplified homogeneous model presented in Eq. (1) and the full bi-layer model in Eq. (2) yield virtually indistinguishable results for diffusivity estimation, validating the physical consistency of both approaches in the current experimental conditions.

### 2.2 Microstructure in MgAZ31 alloy

Magnesium has a hexagonal close-packed (hcp) crystal structure characterised by pronounced mechanical and thermal anisotropy. This mechanical anisotropy, which becomes more evident following plastic deformation processes such as rolling, is primarily due to the preferential orientation of the crystal structure—specifically, the alignment of basal and non-basal planes, the latter being further classified as prismatic and pyramidal. In thin sheet configurations, thermal treatments such as annealing promote the exposure of non-basal planes in the through-thickness direction, along with a reduction in basal plane exposure and a concurrent increase in grain size [10,11]. As a result, annealing affects not only mechanical properties such as hardness but also the intrinsic anisotropy of the alloy.

As well described in recent research by Lv et al. [34], this anisotropy leads to a strong dependence of thermal conductivity on the crystallographic grain orientation, with a reported difference of approximately 30% between conductivity along basal planes and that along non-basal planes, where it is lower. Consequently, when the orientation of the crystal structure changes, thermal conductivity also changes significantly due to the shift in the preferred pathways for heat transport by electrons and phonons. In magnesium, even slight variations in alloy composition or the presence of atoms in a solid solution can introduce significant lattice distortions, reducing the mean free path of electrons and phonons and thereby impacting thermal conductivity. Secondary phases—especially those coherent or semi-coherent with the matrix—introduce local distortions and stress fields that significantly influence the thermal conductivity of magnesium and its alloys. Therefore, changes in the distribution and size of these phases can lead to substantial variations in thermal diffusivity.

Unlike steels, where free electrons predominantly govern heat conduction, the phonon contribution becomes significant in metals with strong lattice distortions, such as magnesium. As a result, even minor distortions or microstructural variations can influence the phononic component of thermal diffusivity since free electrons are less sensitive to minor microstructural changes than phonons.

## 3. Materials and methods

This section describes the specimens used in the experimental phase, including the heat treatment methods employed to modify their mechanical properties. Furthermore, the thermographic setup used for pulsed laser spot thermography tests will be described, followed by an account of the metallographic analyses and subsequent mechanical testing.

### 3.1 Specimens

A total of eight Mg AZ31-H24 specimens with a nominal thickness of 1 mm and approximate dimensions of 70 mm × 70 mm were considered in this study (Figure *1*), as summarized in Table *1*. Three specimens were left in the as-received condition and labeled with the letter A, while the remaining five were thermally treated at 450 °C for 10000 seconds and labeled with the letter C. The thermal treatment was intended to obtain a uniform microstructure throughout the volume and a predicted average grain size, which, according to the equation proposed by Carpenter et al. [39], is expected to reach approximately 12.38 μm.

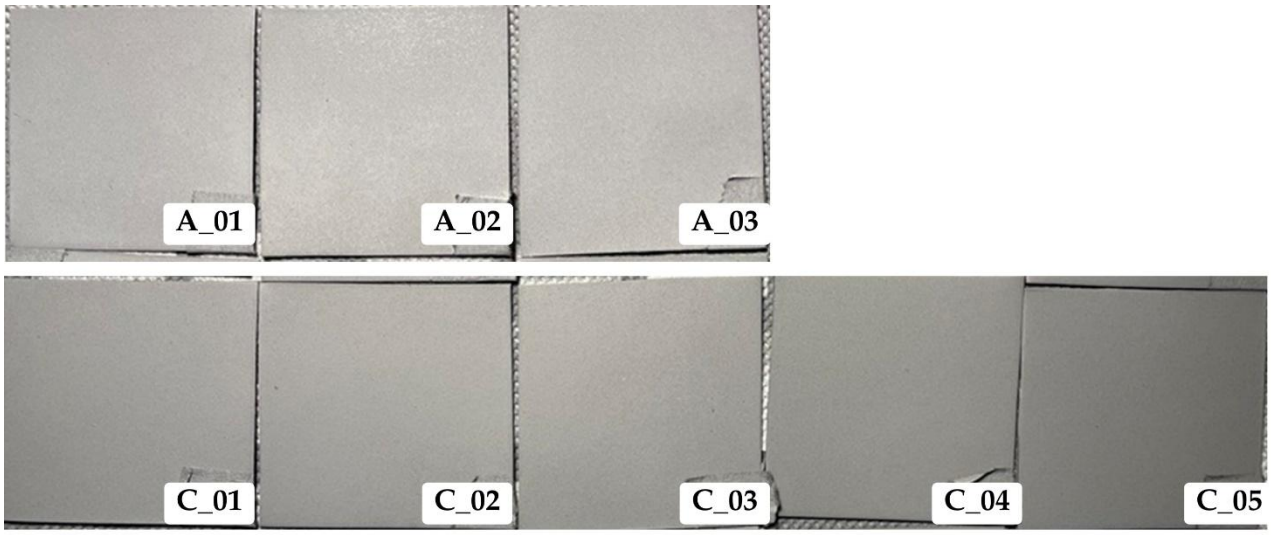


Figure 1. Analysed specimens with graphite coating, A as received state and C annealed.

Table 1. Summary table of the investigated specimens

| ID | Material | State | Nom. Thickness | Meas. Thickness |
|---|---|---|---|---|
| A 01/02/03 | Mg Az 31 – H24 | As received | 1 mm | 0.96 ± 0.30 mm |
| C 01/02/03/04/05 | Mg Az 31 – H24 | Annealed | 1 mm | 0.94 ± 0.40 mm |

The division into three untreated and five treated samples was chosen based on the uniformity of the as-received material condition, which was ensured during the supply phase. Therefore, more replicates were assigned to the annealed group to gather a more extensive dataset on the variability introduced by the heat treatment process.

Based on the theoretical considerations discussed in the previous section, the annealing treatment is expected to promote grain growth and reduce grain boundaries and phonon scattering, thus increasing thermal conductivity in all directions.

Due to the high reflectivity of the surface, the inspected face of each specimen was coated with a thin layer of graphite spray to enhance and homogenize emissivity and improve energy absorption.

### 3.2 Experimental setup

The annealing treatment was performed under atmospheric conditions using a furnace (Nabertherm N 61/H) equipped with three-sided heating and lightweight refractory bricks.

The thermographic setup used for thermal diffusivity measurements was configured in reflection mode, as anticipated in the theoretical section. Specifically, each specimen's graphite-coated surface was heated for 160 μs using a pulsed laser at 1064 nm, with a top-hat distribution and a nominal spot diameter of 10 mm, delivering an energy of approximately 1.5 J. The laser beam was incident at an angle of approximately 15° concerning the surface normal, as illustrated in the setup diagram (Figure *2*). Such an inclination has a negligible influence on the low-angle diffusivity measurement.

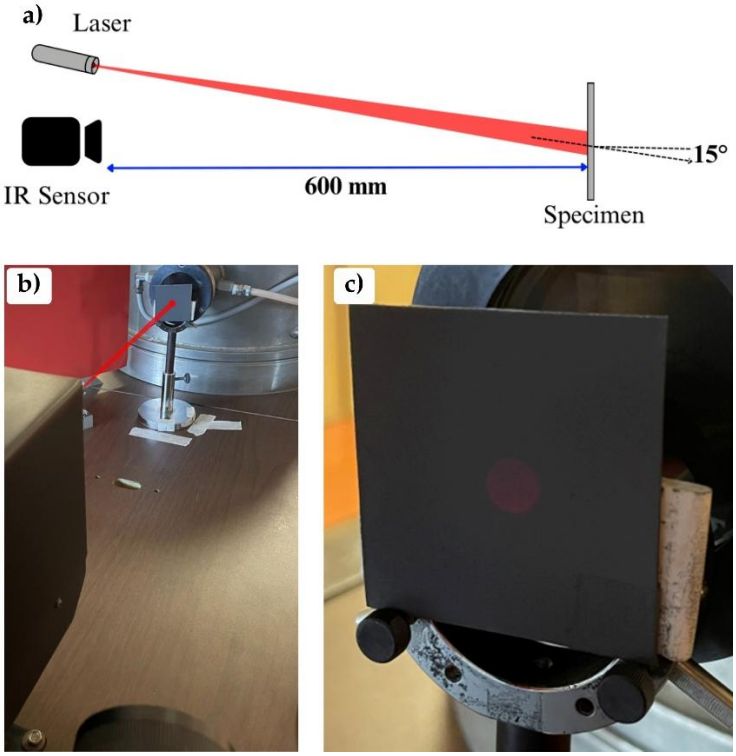


Figure 2 . a) Schematic representation of the experimental set-up adopted. b) Photograph of the experimental set-up adopted. c) Inspection area and laser spot size.

A front-facing FLIR X6981 LW (7.5–9.5 μm) cooled infrared camera was positioned perpendicular to the specimen surface to avoid perspective distortions (Figure *2*). The camera was equipped with a 50 mm lens, resulting in a spatial resolution of 0.25 mm/pixel. Data acquisition was carried out at 7990 Hz, recording the heating and cooling phases for a total acquisition time of about 1 second. This high acquisition frequency was achieved by reducing the acquisition window to 65×125 pixels and selecting a calibration temperature range of –20 °C to 150 °C

For hardness analysis and metallographic measurements, a fully automatic microhardness tester (Qness Q10A+, Salzburg, Austria) and a light microscope (Inverted Microscope Nikon MA200) were used, respectively.

### 3.3 Methods

Each specimen was tested using pulsed laser spot thermography to measure its thermal diffusivity, repeating the test five times. As discussed in the theoretical section, this method allows for evaluating both in-plane and through-thickness thermal diffusivity. Nonetheless, the present work focused on through-thickness measurements alone, even though magnesium exhibits a certain degree of anisotropy due to its crystallographic structure, as described in the related theory section. This choice is justified by previous studies [34], which confirmed the uniformity of the microstructure along the thickness after the applied thermal treatment. Therefore, it is reasonable to assume that the microstructure, grain size, and thermal diffusivity are homogeneous throughout the specimen thickness.

For the analysis of each test, a consistent area of 15x15 $mm^2$ was selected, centred on the laser spot for all acquisitions. As the theoretical section outlines, once a surface region is defined, the temperature signal is spatially integrated over that area. This produces a response equivalent to the one-dimensional (1D) case [48]. This approach offers significant advantages: the integrated signal remains unaffected by the non-uniformity even if the initial temperature distribution is not perfectly uniform—such as a Gaussian profile. Consequently, the thermal diffusivity can be reliably estimated using the 1D model, regardless of minor inhomogeneities in the laser spot.

For each analysis, a fixed temporal window of 0.0365 seconds was used. This time window was selected based on the shape of the thermal response on a log-log scale. Precisely, it needed to be long enough to reach the plateau typical of finite-thickness behaviour but short enough to avoid the onset of heat losses. The exact time window was applied consistently across all tests. Figure *3* shows a representative temperature-time curve obtained experimentally, highlighting the selected analysis window.

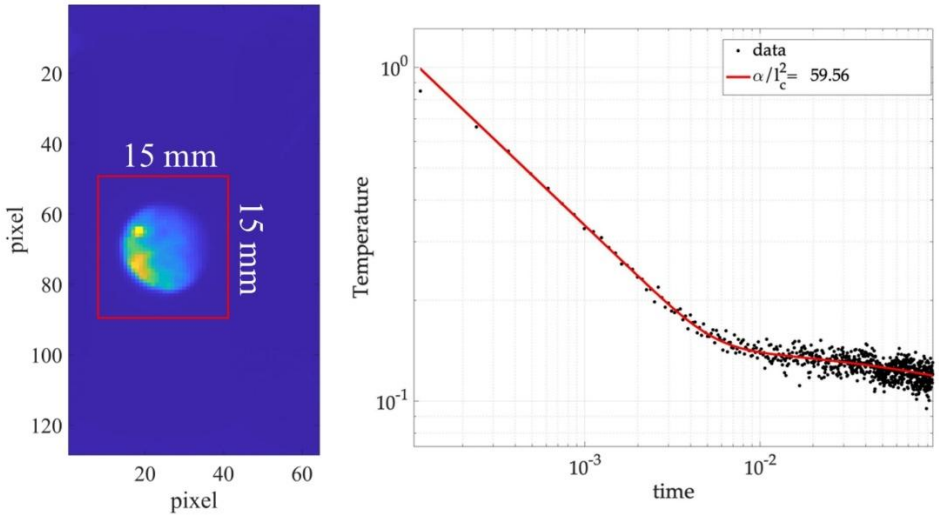


Figure 3. Region of interest (15 × 15 mm²) used for data integration and curve fitting, overlaid on the thermogram acquired at t = 0.125 ms after the peak temperature. The selected area fully encompasses the thermally affected zone during the time window used for diffusivity estimation. Experimental temperature-time curve (black dots) obtained by averaging over the selected area, and corresponding fit (red curve) based on the analytical model used to extract the $\alpha/L^2$ parameter.

Subsequently, hardness tests were performed on the specimens to verify the effectiveness of the thermal treatment, along with metallographic analyses aimed at measuring the average grain size of each sample and comparing it to the predicted value according to the equation proposed by Carpenter et al. [39].
Before the analyses, each sample was cut, hot mounted, ground, polished and etched by immersion for 5 s in acetic-picral solution (5 ml acetic acid, 6 g picric acid, 10 ml water, 100 ml ethanol).
Then, the microstructure of each sample was observed through its thickness. According to the ASTM E112-13 (2021) standard, the Heyn Lineal Intercept procedure was applied to measure the average size of the grains.
Vickers microhardness tests were then performed on the same samples in accordance with the EN ISO 6507-1:2023 standard. The Vickers microhardness (load=100 gf, holding time=5 s) was measured along a five-points path located at half of the sample's thickness.
The specimen thickness was also determined through optical microscopy. This step was necessary since the pulsed laser spot method is susceptible to thickness variations, making precise thickness measurements critical for accurate diffusivity calculation. To ensure the reliability of the calculated thermal diffusivity, multiple local thickness measurements were performed on each sample cross-section. The specimens were prepared with careful polishing to allow clear identification of boundary interfaces under optical microscopy. The methodology thus assumes that thickness is known with sufficient accuracy, which can be achieved under controlled laboratory conditions but may be more difficult in real-world applications with unmachined surfaces or strong geometrical variability. The measured thickness values were then used to calculate thermal diffusivity for each sample.

The same procedure was applied to the untreated (as-received) specimens. First, the thermal diffusivity values were compared with the corresponding hardness values to investigate the correlation between the two properties. Then, the average grain size of each specimen was measured. A statistical approach was adopted to assess the relationship between hardness, grain size, and thermal diffusivity.

In Figure *4* is summarised the proposed procedure adopted.

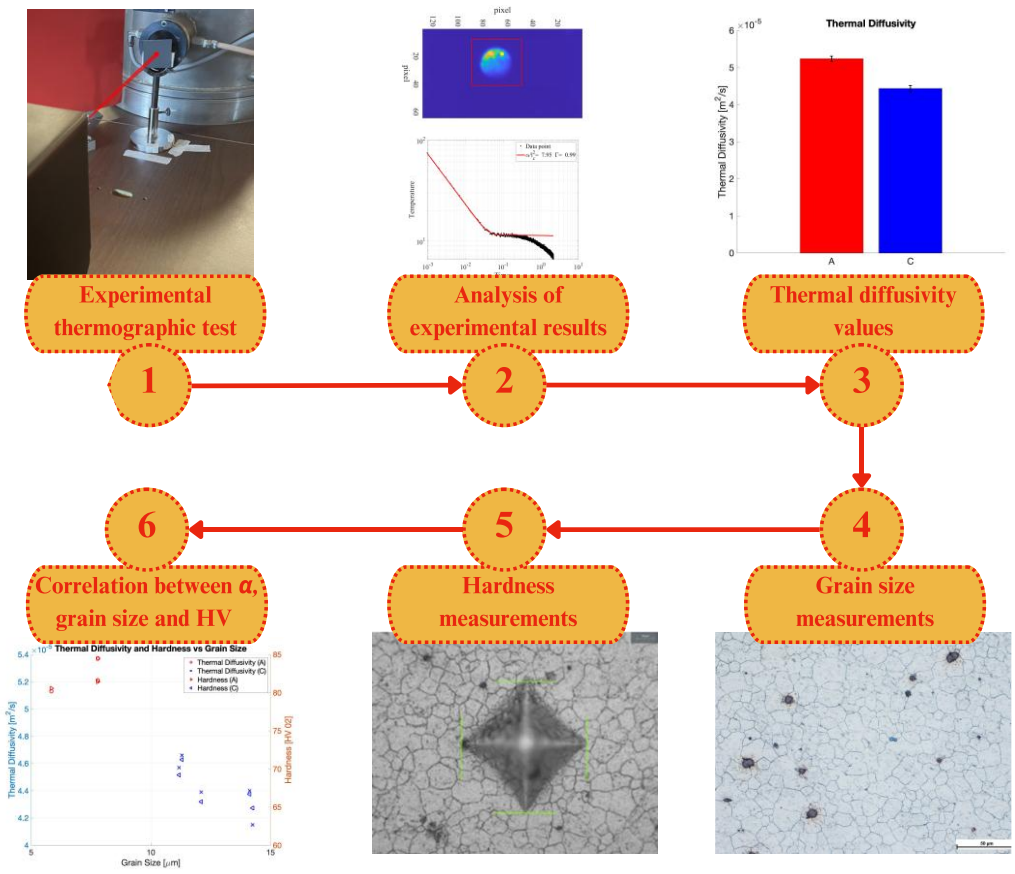


Figure 4. Summary diagram of the proposed procedure.

## 4. Results and discussion

Figure *5* shows two representative experimental curves obtained from two groups of specimens. Each curve corresponds to a sample group, highlighting a different thermal behaviour between the two microstructures. Although the nominal thickness of all analysed specimens was the same, microscopic measurements revealed slight differences. For this reason, even if the two thermal response curves do not differ significantly in shape, each sample's specific thickness must be considered.

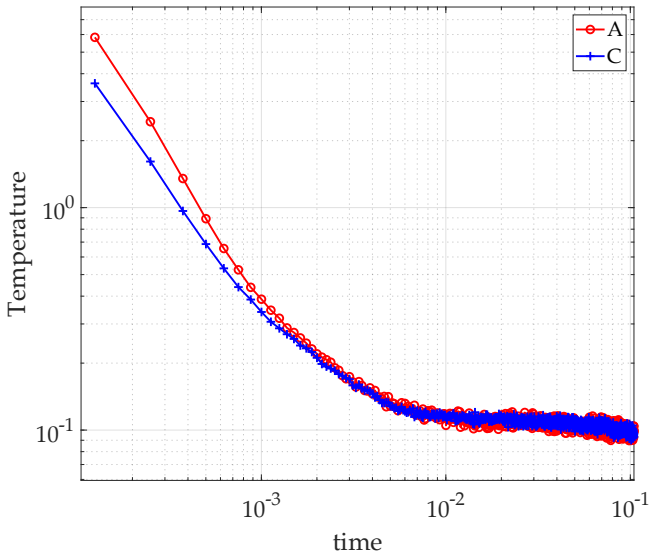


Figure 5. Two experimental curves obtained from the thermographic tests: in red, the curve corresponding to the specimens in the as-received state, and in blue, the curve corresponding to the annealed state.

As previously discussed, the parameter that can be extracted from the thermographic analysis is the ratio $\alpha/L^2$, where $\alpha$ is the through-thickness thermal diffusivity and $L$ is the specimen thickness. Table *2* reports the values of this parameter obtained for each measurement, including the associated uncertainties.

Table 2 Summary table of thermographic results with the $\alpha/L^2$ parameter obtained for each specimen.

| ID | State | Repetitions | $\alpha/L^2$ $[1/s]$ |
|---|---|---|---|
| A 01 | As received | 5 | 56.48 ± 1.74 |
| A 02 | As received | 5 | 55.86 ± 0.55 |
| A 03 | As received | 5 | 55.67 ± 1.33 |
| C 01 | Annealed | 5 | 50.79 ± 1.27 |
| C 02 | Annealed | 5 | 49.05 ± 1.76 |
| C 03 | Annealed | 5 | 52.71 ± 2.56 |
| C 04 | Annealed | 5 | 49.79 ± 0.71 |
| C 05 | Annealed | 5 | 51.78 ± 1.27 |

Figure 6 shows two representative micrographs of the specimens from the as received and annealed groups. The annealing treatment increased the average grain size, with the values summarized in Table *3*. Additionally, the thicknesses of each specimen were extracted from the same microscopy analysis.

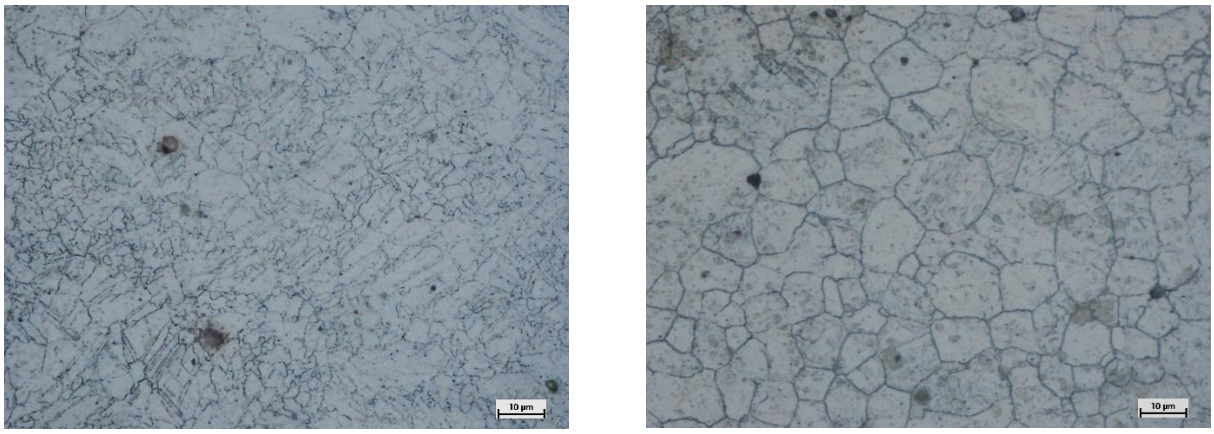


a) b)

Figure 6 Representative micrographs of the specimens from the a) as received and b) annealed groups; scale bar: 10 µm

Figure 7 displays a few examples of the hardness indentations used to obtain the values summarized in Table *3*. From the measured grain sizes and hardness values, it is possible to confirm the effectiveness of the annealing treatment, as the final grain size is consistent with the estimate based on the equation proposed by Carpenter et al.[39].

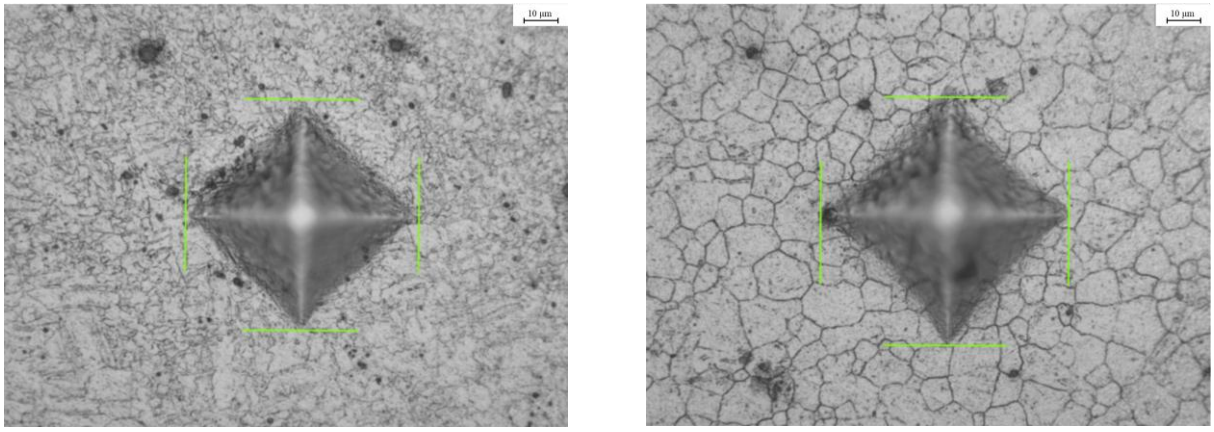

a) b)

Figure 7 Representative images of the indentation after hardness tests of the specimens from the a) as received and b) annealed groups; scale bar: 10 μm

The average grain size in the as-received MgAZ31-H24 specimens was 7.14 ± 0.92 μm, while after annealing, it increased to 12.59 ± 1.34 μm, corresponding to an approximate 75% increase. The mechanical properties also evolved as expected, with hardness decreasing from 81.16 ± 1.68 HV0.2 to 67.54 ± 2.35 HV0.2, a reduction of approximately 13%.

Using the thickness values measured for each specimen, it was then possible to calculate the thermal diffusivity in the through-thickness direction based on the previously obtained $a/L^2$ ratios. The results are summarized in Table *3*. As shown in Figure *8* and reported in Table *3*, the specimens that underwent annealing (group C) exhibited a reduction in through-thickness thermal diffusivity compared to the as-received MgAZ31-H24 group. Specifically, a reduction of about 18% was observed.

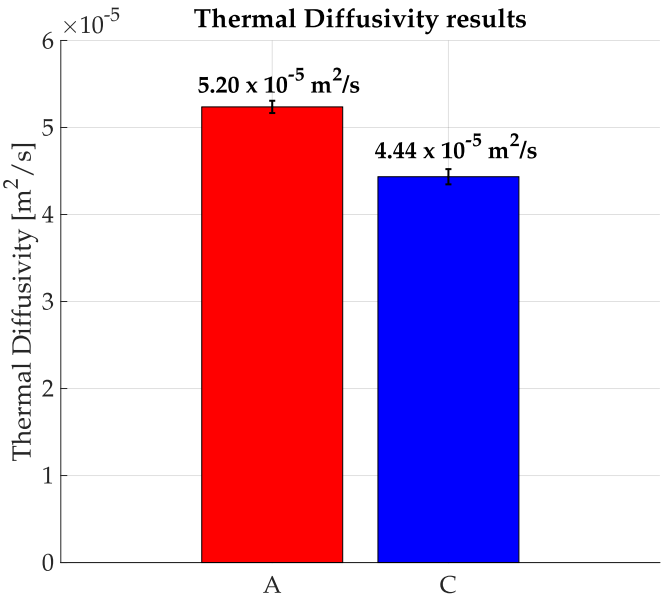


Figure 8 Histogram of average thermal diffusivity measurements for the as-received (A) and annealed (C) specimens.

Table 3. Summary table of experimental results for hardness, grain size, and thermal diffusivity for each specimen.

| ID | State | Repetitions | Hardness [HV 02] | Grain size [μm] | Thermal diffusivity [x $10^{-5}$ $m^2/s$] |
|---|---|---|---|---|---|
| A 01 | As received | 5 | 80.56 | 5.85 ± 0.24 | 5.21 ± 0.16 |
| A 02 | As received | 5 | 81.44 | 7.79 ± 0.69 | 5.26 ± 0.05 |

| | | | | | |
|---|---|---|---|---|---|
| A 03 | As received | 5 | 84.48 | 7.79 ± 0.75 | 5.13 ± 0.12 |
| C 01 | Annealed | 5 | 66.70 | 14.12 ± 1.11 | 4.39 ± 0.11 |
| C 02 | Annealed | 5 | 71.22 | 11.30 ± 0.88 | 4.15 ± 0.15 |
| C 03 | Annealed | 5 | 62.22 | 11.19 ± 0.76 | 4.66 ± 0.12 |
| C 04 | Annealed | 5 | 64.88 | 14.25 ± 2.36 | 4.40 ± 0.06 |
| C 05 | Annealed | 5 | 65.70 | 12.11 ± 1.24 | 4.58 ± 0.11 |

The statistical analysis revealed a significant negative correlation between grain size and thermal diffusivity, as indicated by Pearson's correlation coefficient ($R = -0.907$, $p < 0.01$), suggesting that smaller grain sizes correspond to higher thermal diffusivity. Additionally, a relevant positive correlation was observed between HV 02 hardness and thermal diffusivity ($R = 0.745$, $p < 0.05$), indicating that samples with higher hardness exhibit greater thermal diffusivity, thus highlighting a positive correlation.

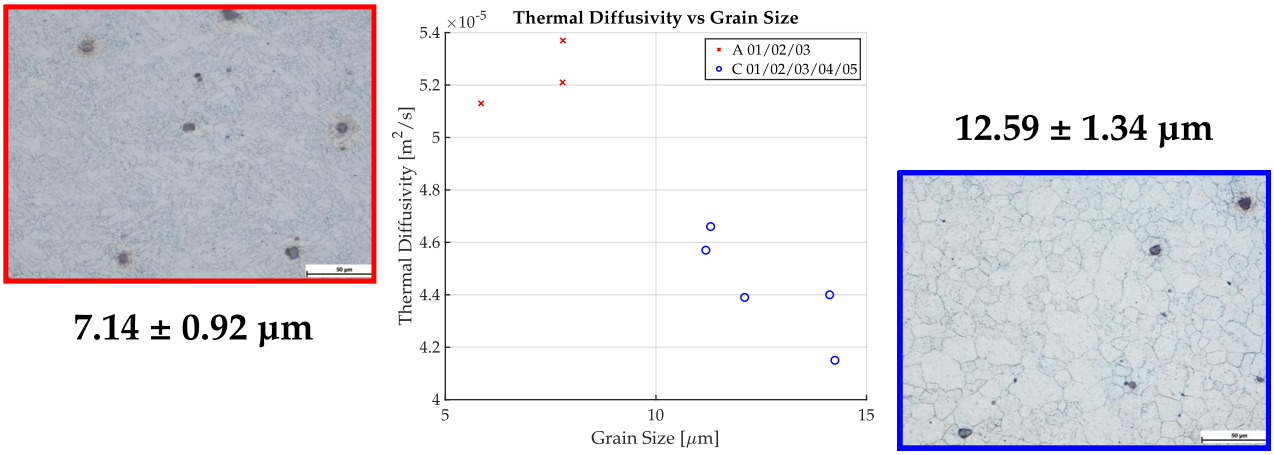


Figure 9. Plot of thermal diffusivity vs. grain size for each specimen, with examples of grain size for the as-received (red square) and annealed (blue square) states.

Despite the increase in grain size —which typically leads to a reduction in grain boundary scattering and, therefore, higher thermal diffusivity—the observed diffusivity decreased, indicating that the expected inverse correlation between hardness and diffusivity observed in steels does not apply here, as it is clearly visible in Figure *9* and Figure *10* and resumed in the graphic in Figure *11*. Several concurrent phenomena induced by annealing must be considered in magnesium alloys, making the interpretation of thermal diffusivity variations less straightforward.

One key factor is the crystallographic texture. As discussed in the theoretical section, magnesium has a hexagonal close-packed (hcp) structure, which inherently leads to mechanical and thermal anisotropy. Thermal conductivity along basal planes is at least 30% higher than along non-basal planes [34], meaning that the grain orientation concerning the direction of heat flow plays a significant role in determining thermal transport properties. In the as-received MgAZ31-H24 condition, basal planes are expected to be predominantly aligned parallel to the surface. In contrast, through the thickness, prismatic and pyramidal planes and mixed orientations are present. Annealing induces grain reorientation—partly due to twinning and the reduction of internal energy—leading to greater exposure of non-basal planes in the through-thickness direction and a weakening of the initial basal texture [34].

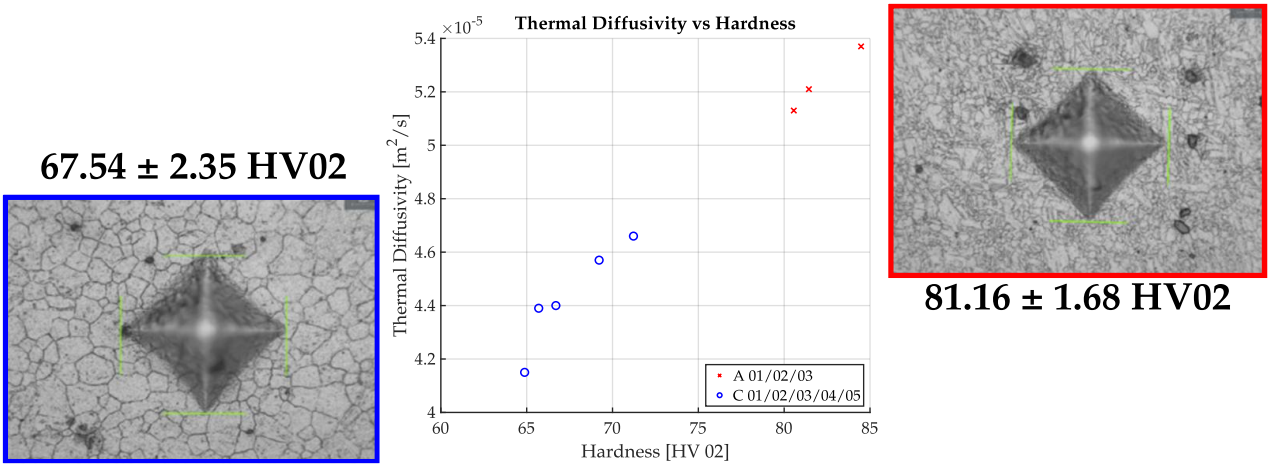


Figure 10. Plot of thermal diffusivity vs. hardness HV02 for each specimen, with examples of indenter imprint for the as-received (red square) and annealed (blue square) states.

Another plausible explanation for the observed decrease in thermal diffusivity after annealing is the formation or growth of precipitates. These secondary phases, primarily if coherent or semi-coherent with the matrix, act as scattering centres for phonons and electrons, impeding heat flow. Solid solution atoms and dislocations can also play a role: the former mainly disturb electronic conduction, while the latter act as barriers to phononic and electronic transport [34].

Altogether, these microstructural phenomena contribute to the reduction of thermal diffusivity in magnesium alloys, counteracting the effect of grain growth that would otherwise increase it. Since these mechanisms have opposing effects, the experimental results suggest that the so-called "secondary" mechanisms—texture evolution, precipitation, solid solution formation, and dislocation density—significantly impact heat transport properties more than grain size alone. This indicates that thermal diffusivity in the magnesium alloy studied is particularly sensitive to such microstructural features, making it a suitable indicator for assessing the presence and evolution of these effects.

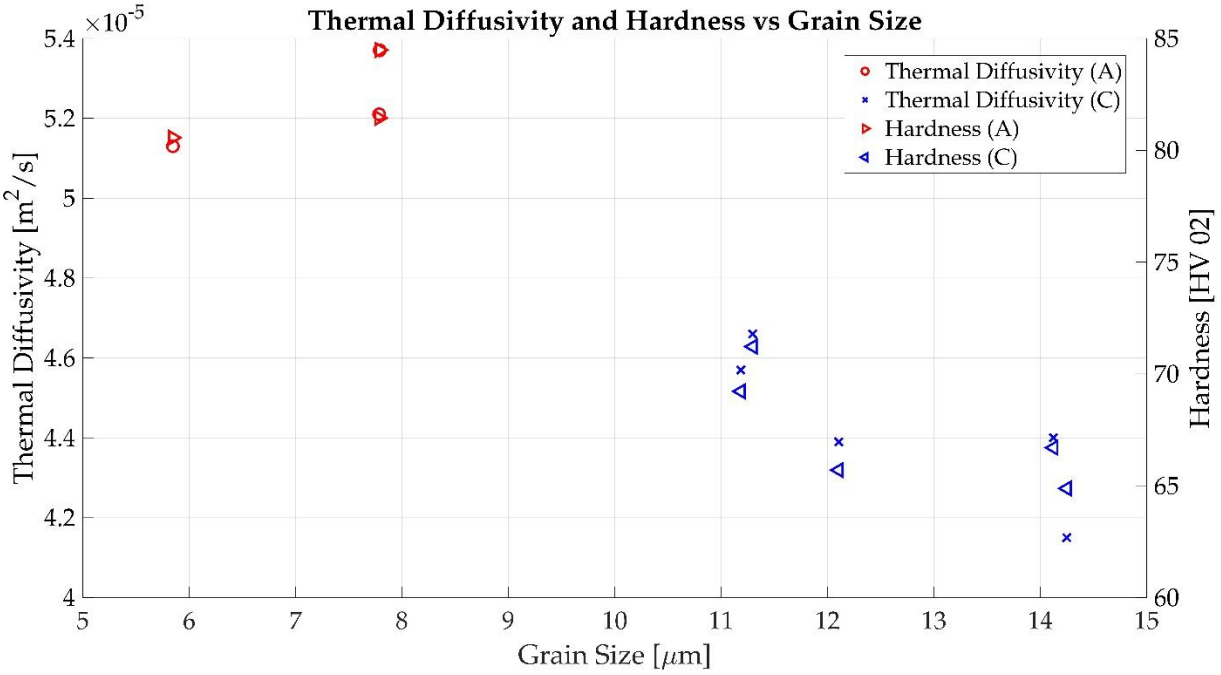


Figure 11. Plot of thermal diffusivity vs. grain size and hardness vs. grain size.

## 5. Conclusions

In this work, the effectiveness of pulsed laser spot thermography in evaluating the impact of annealing treatment on MgAZ31-H24 was investigated, focusing on detecting microstructural variations through through-thickness thermal diffusivity measurements.

Eight MgAZ31-H24 specimens were analysed: three in the as-received condition and five subjected to annealing at 450 °C for 10000 s. Each specimen was tested to measure thermal diffusivity and assess its correlation with the microstructural changes induced by the heat treatment. Mechanical hardness testing and grain size measurements were then conducted to verify the success of the annealing process using conventional methods. These tests confirmed a reduction in hardness of approximately 13% and an increase in average grain size of about 75%. However, thermal diffusivity decreased by approximately 18% after annealing.

This result challenges the commonly observed inverse correlation between hardness and thermal diffusivity in metals like steel. In the case of the magnesium alloy investigated, the effect of grain growth—typically associated with reduced phonon scattering and increased thermal transport—appears to be outweighed by other microstructural factors. In particular, crystallographic texture evolution, the formation of secondary phases, dislocations, and solute atoms in solid solutions will likely play a dominant role in limiting heat diffusion.

Although these phenomena were not directly observed in the present study, prior literature on hcp metals and the known effects of annealing support this interpretation. Specifically, after annealing, the exposure of prismatic and pyramidal planes in the through-thickness direction increases. At the same time, intermediate orientations are reduced, weakening the basal texture that characterizes the as-received condition. Since basal planes in hcp magnesium exhibit higher thermal conductivity than non-basal ones, this texture evolution likely contributes to the observed reduction in diffusivity. Additional scattering mechanisms, such as those induced by precipitates, dislocations and solid solution atoms, further reduce thermal transport.

These findings demonstrate that thermal diffusivity in magnesium alloys is highly sensitive to complex microstructural features beyond grain size alone. Therefore, thermal diffusivity—measured via non-destructive thermographic methods—can serve as an effective indicator for assessing such features. It is important to note that the present method requires a known and reasonably uniform specimen thickness. While this assumption holds in the current experimental conditions, its applicability to components with variable thickness may be more difficult. Future developments should therefore consider the integration of auxiliary thickness mapping or the use of inversion approaches robust to geometric uncertainty.

To expand the applicability of the proposed method, further investigations are required to explore the sensitivity of thermographic measurements to variations in texture, precipitation, and solid solution. In particular, the following future steps are proposed:

- Perform a comprehensive characterization of specimens subjected to different annealing durations to identify the point at which grain growth effects on conductivity become negligible compared to other microstructural factors.
- Conduct detailed analyses using SEM, EBSD, EDS, and XRD to determine the dominant mechanisms responsible for conductivity reduction after annealing. Based on these findings, develop a predictive model that accounts for such effects to estimate mechanical properties from thermal diffusivity data obtained via thermography.

These developments would pave the way for using thermal diffusivity as a reliable, non-destructive indicator of microstructural state and mechanical performance in magnesium alloys.

## Acknowledgments

The activities have been financed by the European Union - NextGenerationEU (National Sustainable Mobility Center CN00000023, Italian Ministry of University and Research Decree n. 1033 - 17/06/2022, Spoke 11 - Innovative Materials & Lightweighting). The opinions expressed are those of the authors only and should not be considered as representative of the European Union or the European Commission's official position. Neither the European Union nor the European Commission can be held responsible for them.

## Author contributions

**Giuseppe Dell'Avvocato:** conceptualization, methodology, validation, investigation, visualization, formal analysis, writing - original draft, writing - review and editing. **Angela Cusanno**: conceptualization, methodology,

validation, investigation, writing - review and editing. **Paolo Bison**: software, validation, investigation, supervision, writing - review and editing. **Stefano Rossi:** formal analysis, investigation, writing - review and editing. **Gianfranco Palumbo**: supervision, resources, funding acquisition, writing - review and editing. **Giovanni Ferrarini**: methodology, investigation, resources, supervision, writing - review and editing.

## Disclosure statement

The authors report there are no competing interests to declare.

## References


[1] Liu B, Yang J, Zhang X, Yang Q, Zhang J, Li X. Development and application of magnesium alloy parts for automotive OEMs: A review. Journal of Magnesium and Alloys 2023;11:15–47. https://doi.org/10.1016/j.jma.2022.12.015.

[2] Akbarzadeh FZ, Sarraf M, Ghomi ER, Kumar VV, Salehi M, Ramakrishna S, et al. A state-of-the-art review on recent advances in the fabrication and characteristics of magnesium-based alloys in biomedical applications. Journal of Magnesium and Alloys 2024;12:2569–94. https://doi.org/10.1016/j.jma.2024.06.015.

[3] Singh J, Wahab Hashmi A, Ahmad S, Tian Y. Critical review on biodegradable and biocompatibility magnesium alloys: Progress and prospects in bio-implant applications. Inorg Chem Commun 2024;169. https://doi.org/10.1016/j.inoche.2024.113111.

[4] Chen Y, Zhang S, Bai J, Yang Y, Wang Y, Zhou Y, et al. Magnesium-based biomaterials for coordinated tissue repair: A comprehensive overview of design strategies, advantages, and challenges. Journal of Magnesium and Alloys 2024. https://doi.org/10.1016/j.jma.2024.05.028.

[5] Šašek S, Minárik P, Stráská J, Hosová K, Veselý J, Kubásek J, et al. Novel Ultrafine-Grain Mg-Gd/Nd-Y-Ca Alloys with an Increased Ignition Temperature. Materials 2023;16:1299. https://doi.org/10.3390/ma16031299.

[6] Sorgente D, Palumbo G, Scintilla LD, Tricarico L. Gas forming of an AZ31 magnesium alloy at elevated strain rates. The International Journal of Advanced Manufacturing Technology 2016;83:861–72. https://doi.org/10.1007/s00170-015-7614-0.

[7] Blala H, Pengzhi C, Shenglun Z, Khan S. Evolution of hot metal gas forming (HMGF) technologies and its applications: a review. The International Journal of Advanced Manufacturing Technology 2024;131:3441–66. https://doi.org/10.1007/s00170-024-13289-1.

[8] Zhang KF, Wang GF, Wu DZ, Wang ZR. Research on the controlling of the thickness distribution in superplastic forming. J Mater Process Technol 2004;151:54–7. https://doi.org/10.1016/j.jmatprotec.2004.04.008.

[9] Cusanno A, Guglielmi P, Sorgente D, Palumbo G. Numerical/experimental investigation of the effect of the laser treatment on the thickness distribution of a magnesium superplastically formed part. Adv Manuf 2024. https://doi.org/10.1007/s40436-024-00497-x.

[10] Kaya AA. A Review on Developments in Magnesium Alloys. Front Mater 2020;7. https://doi.org/10.3389/fmats.2020.00198.

[11] Mishra SK, Tiwari SM, Carter JT, Tewari A. Texture evolution during annealing of AZ31 Mg alloy rolled sheet and its effect on ductility. Materials Science and Engineering: A 2014;599:1–8. https://doi.org/10.1016/j.msea.2014.01.034.

[12] Lin B, Zhang H, Meng Y, Wang L, Fan J, Zhang S, et al. Deformation behavior, microstructure evolution, and dynamic recrystallization mechanism of an AZ31 Mg alloy under high-throughput gradient thermal compression. Materials Science and Engineering: A 2022;847. https://doi.org/10.1016/j.msea.2022.143338.

[13] Guo E, Du Z, Chen X, Chen Z, Kang H, Cao Z, et al. Development of magnesium alloys: Advanced characterization using synchrotron radiation techniques. J Mater Sci Technol 2024;195:93–110. https://doi.org/10.1016/j.jmst.2024.01.029.

[14] Lu L, Huang JW, Fan D, Bie BX, Sun T, Fezzaa K, et al. Anisotropic deformation of extruded magnesium alloy AZ31 under uniaxial compression: A study with simultaneous in situ synchrotron x-ray imaging and diffraction. Acta Mater 2016;120:86–94. https://doi.org/10.1016/j.actamat.2016.08.029.

[15] Kumar R, Lhuissier P, Villanova J, Salvo L, Blandin JJ. Elementary growth mechanisms of creep cavities in AZ31 alloy revealed by in situ X-ray nano-tomography. Acta Mater 2022;228. https://doi.org/10.1016/j.actamat.2022.117760.

[16] Durdu S, Bayramoglu S, Demirtaş A, Usta M, Üçşk AH. Characterization of AZ31 Mg Alloy coated by plasma electrolytic oxidation. Vacuum 2013;88:130–3. https://doi.org/10.1016/j.vacuum.2012.01.009.

[17] Groz MM, Abisset-Chavanne E, Batsale JC, Sommier A. Active thermal super-resolution based on laser flying spot technique coupled with IR thermography and wavelet transform. Quant Infrared Thermogr J 2024:1–24. https://doi.org/10.1080/17686733.2023.2299499.

[18] D'Accardi E, Dell'Avvocato G, Masciopinto G, Marinelli G, Fumarola G, Palumbo D, et al. Evaluation of typical rail defects by induction thermography: experimental results and procedure for data analysis during high-speed laboratory testing. Quant Infrared Thermogr J 2024:1–22. https://doi.org/10.1080/17686733.2024.2340060.

[19] Hsiao T-Y, Sfarra S, Liu Y, Yao Y. Two-dimensional Hilbert-Huang transform-based thermographic data processing for non-destructive material defect detection. Quant Infrared Thermogr J 2024:1–16. https://doi.org/10.1080/17686733.2024.2379066.

[20] Oswald-Tranta B. Inductive thermography – review of a non-destructive inspection technique for surface crack detection. Quant Infrared Thermogr J 2025:1–25. https://doi.org/10.1080/17686733.2024.2448049.

[21] Helvig K, Trouvé-Peloux P, Gaverina L, Abeloos B, Roche J-M. Automated crack detection on metallic materials with flying-spot thermography using deep learning and progressive training. Quant Infrared Thermogr J 2025;22:21–40. https://doi.org/10.1080/17686733.2023.2266176.

[22] Santoro L, Razza V, De Maddis M. Frequency-based analysis of active laser thermography for spot weld quality assessment. International Journal of Advanced Manufacturing Technology 2024;130:3017–29. https://doi.org/10.1007/s00170-023-12845-5.

[23] Lecompagnon J, Hirsch PD, Rupprecht C, Ziegler M. Nondestructive thermographic detection of internal defects using pixel-pattern based laser excitation and photothermal super resolution reconstruction. Sci Rep 2023;13. https://doi.org/10.1038/s41598-023-30494-2.

[24] D'Accardi E, De Finis R, Dell'Avvocato G, Masciopinto G, Palumbo D, Galietti U. Conduction thermography for non-destructive assessment of fatigue cracks in metallic materials. Infrared Phys Technol 2024;140:105394. https://doi.org/10.1016/j.infrared.2024.105394.

[25] D'Accardi E, Chiappini F, Giannasi A, Guerrini M, Maggiani G, Palumbo D, et al. Online monitoring of direct laser metal deposition process by means of infrared thermography. Progress in Additive Manufacturing 2024;9:983–1001. https://doi.org/10.1007/s40964-023-00496-7.

[26] Oster S, Breese PP, Ulbricht A, Mohr G, Altenburg SJ. A deep learning framework for defect prediction based on thermographic in-situ monitoring in laser powder bed fusion. J Intell Manuf 2024;35:1687–706. https://doi.org/10.1007/s10845-023-02117-0.

[27] AbouelNour Y, Gupta N. Assisted defect detection by in-process monitoring of additive manufacturing using optical imaging and infrared thermography. Addit Manuf 2023;67:103483. https://doi.org/10.1016/j.addma.2023.103483.

[28] Dell'Avvocato G, Palumbo D, Galietti U. A non-destructive thermographic procedure for the evaluation of heat treatment in Usibor®1500 through the thermal diffusivity measurement. NDT and E International 2023;133. https://doi.org/10.1016/j.ndteint.2022.102748.

[29] Dell'Avvocato G, Bison P, Palmieri ME, Ferrarini G, Palumbo D, Tricarico L, et al. Non-destructive estimation of mechanical properties in Usibor® 1500 via thermal diffusivity measurements: A thermographic procedure. NDT and E International 2024;143. https://doi.org/10.1016/j.ndteint.2023.103034.

[30] Zaeimi M, De Finis R, Palumbo D, Galietti U. Fatigue limit estimation of metals based on the thermographic methods: A comprehensive review. Fatigue Fract Eng Mater Struct 2024;47:611–46. https://doi.org/10.1111/ffe.14206.

[31] Pathak P, Gururaja S, Kumar V, Nuttall D, Mahmoudi A, Khonsari MM, et al. Examining infrared thermography based approaches to rapid fatigue characterization of additively manufactured compression molded short fiber thermoplastic composites. Compos Struct 2025;351:118610. https://doi.org/10.1016/j.compstruct.2024.118610.

[32] Liu Y, Baddour N, Mandelis A. Transverse depth-profilometric hardness photothermal phase imaging of heat treated steels. J Appl Phys 2003;94:5543–8. https://doi.org/10.1063/1.1613808.

[33] Walther HG, Fournier D, Krapez JC, Luukkala M, Schmitz B, Sibilia C, et al. Photothermal Steel Hardness Measurements-Results and Perspectives. n.d.

[34] Lv H, Tan J, Yuan Q, Wang F, Zhou Y, Dong Q, et al. Recent advancements in thermal conductivity of magnesium alloys. Journal of Magnesium and Alloys 2024;12:1687–708. https://doi.org/10.1016/j.jma.2024.02.007.

[35] Bison P, Cernuschi F, Capelli S. A thermographic technique for the simultaneous estimation of in-plane and in-depth thermal diffusivities of TBCs. Surf Coat Technol 2011;205:3128–33. https://doi.org/10.1016/j.surfcoat.2010.11.013.

[36] Cernuschi F, Bison P, Marinetti S, Campagnoli E. Thermal diffusivity measurement by thermographic technique for the non-destructive integrity assessment of TBCs coupons. Surf Coat Technol 2010;205:498–505. https://doi.org/10.1016/j.surfcoat.2010.07.024.

[37] Cernuschi SAF, Bison PG, Figari A, Marinetti S, Grinzato E. Thermal Diffusivity Measurements by Photothermal and Thermographic Techniques 1. vol. 25. 2004.

[38] Fernandes H, Zhang H, Figueiredo A, Malheiros F, Ignacio LH, Sfarra S, et al. Machine learning and infrared thermography for fiber orientation assessment on randomly-oriented strands parts. Sensors (Switzerland) 2018;18. https://doi.org/10.3390/s18010288.

[39] Carpenter AJ, Antoniswamy AR, Carter JT, Hector LG, Taleff EM. A mechanism-dependent material model for the effects of grain growth and anisotropy on plastic deformation of magnesium alloy AZ31 sheet at 450°C. Acta Mater 2014;68:254–66. https://doi.org/10.1016/j.actamat.2014.01.043.

[40] Salazar A, Colom M, Mendioroz A. Laser-spot step-heating thermography to measure the thermal diffusivity of solids. International Journal of Thermal Sciences 2021;170. https://doi.org/10.1016/j.ijthermalsci.2021.107124.

[41] Colom M, Bedoya A, Mendioroz A, Salazar A. Measuring the in-plane thermal diffusivity of moving samples using laser spot lock-in thermography. International Journal of Thermal Sciences 2020;151. https://doi.org/10.1016/j.ijthermalsci.2020.106277.

[42] Gaverina L, Bensalem M, Bedoya A, González J, Sommier A, Battaglia JL, et al. Constant Velocity Flying Spot for the estimation of in-plane thermal diffusivity on anisotropic materials. International Journal of Thermal Sciences 2019;145. https://doi.org/10.1016/j.ijthermalsci.2019.106000.

[43] Tang H, Melnikov A, Liu M, Sfarra S, Zhang H, Mandelis A. Physics informed neural networks for solving inverse thermal wave coupled boundary-value problems. Int J Heat Mass Transf 2025;245. https://doi.org/10.1016/j.ijheatmasstransfer.2025.126985.

[44] Hng Lim W, Sfarra S, Hsiao TY, Yao Y. Physics-Informed Neural Networks for Defect Detection and Thermal Diffusivity Evaluation in Carbon Fiber Reinforced Polymer using Pulsed Thermography. IEEE Trans Instrum Meas 2025. https://doi.org/10.1109/TIM.2025.3527517.

[45] Ryu M, Batsale JC, Morikawa J. Quadrupole modelling of dual lock-in method for the simultaneous measurements of thermal diffusivity and thermal effusivity. Int J Heat Mass Transf 2020;162. https://doi.org/10.1016/j.ijheatmasstransfer.2020.120337.

[46] Cernuschi F, Russo A, Lorenzoni L, Figari A. In-plane thermal diffusivity evaluation by infrared thermography. Review of Scientific Instruments 2001;72:3988–95. https://doi.org/10.1063/1.1400151.

[47] Sfarra S, Cicone A, Yousefi B, Perilli S, Robol L, Maldague XPV. Maximizing the detection of thermal imprints in civil engineering composites via numerical and thermographic results pre-processed by a groundbreaking mathematical approach. International Journal of Thermal Sciences 2022;177. https://doi.org/10.1016/j.ijthermalsci.2022.107553.

[48] Bison PG, Cernuschi F, Grinzato E, Marinetti S, Robba D. Ageing evaluation of thermal barrier coatings by thermal diffusivity. Infrared Phys Technol 2007;49:286–91. https://doi.org/10.1016/j.infrared.2006.06.019.